Synthesis and Kinetic Adsorption Characteristics of Zeolite/CeO_2 Nanocomposite

Emmanuel Nyankson , Jonas Adjasoo , Johnson Kwame Efavi , Abu Yaya , Gloria Manu , Asare Kingsford , Richard Yeboah Abrokwah

PII: S2468-2276(19)30818-X
DOI: https://doi.org/10.1016/j.sciaf.2019.e00257
Reference: SCIAF 257

To appear in: *Scientific African*

Received date: 13 February 2019
Revised date: 25 October 2019
Accepted date: 19 November 2019

Please cite this article as: Emmanuel Nyankson , Jonas Adjasoo , Johnson Kwame Efavi , Abu Yaya , Gloria Manu , Asare Kingsford , Richard Yeboah Abrokwah , Synthesis and Kinetic Adsorption Characteristics of Zeolite/CeO_2 Nanocomposite, *Scientific African* (2019), doi: https://doi.org/10.1016/j.sciaf.2019.e00257

Highlights

- Preparation and Characterisation of Zeolite / CeO_2 Nanocomposite
- Zeolite / CeO_2 Nanocomposite as a potential adsorbent for waste water treatment
- Adsorption kinetics of Zeolite / CeO_2 Nanocomposite established

Synthesis and Kinetic Adsorption Characteristics of Zeolite / CeO_2 Nanocomposite

Emmanuel Nyankson[1], Jonas Adjasoo[1], Johnson Kwame Efavi[1*], Abu Yaya[1], Gloria Manu[1], Asare Kingsford[2], Richard Yeboah Abrokwah[2]

[1]University of Ghana, School of Engineering Sciences, Department of Materials Science & Engineering, P.O. BOX LG 74

[2]North Carolina A&T State University, Energy and Environmental Systems Department, Greensboro NC 27411

** Corresponding author: Department of Materials Science and Engineering, University of Ghana, Email: jkefavi@ug.edu.gh, Tel., +233-244-111-2*

ABSTRACT

Adsorption is an effective method for treating polluted water bodies. In this study, Zeolite/Cerium oxide nanocomposite (Z/CeO_2-NC) was hydrothermally synthesize and its adsorption capacity on methylene blue organic dye (MB) studied. The as-synthesized nanocomposite (Z/CeO_2–NC) were characterized using X-Ray Diffraction (XRD), Fourier Transform Infra-Red (FT-IR), Energy Dispersive X-Ray Spectroscopy (EDX) and Scanning Electron Microscopy (SEM). Kinetic models and sorption isotherms were used to predict the adsorption rate constants and process mechanisms. The synthesized Z/CeO_2-NC showed an excellent adsorption kinetics of methylene blue and the characteristics of adsorption best fitted a pseudo-second-order model. The rate parameters of other models were evaluated and compared to establish the adsorption mechanisms. The Langmuir isotherm model best fitted the adsorption process indicating a homogeneous monolayer of the dye on the surface of the adsorbent. The thermodynamic Gibbs free energy (ΔG) parameter was determined to be negative, indicating a spontaneous adsorption process. The synthesized Z/CeO_2-NCs showed strong adsorption for methylene blue dye with increasing amount of CeO_2. The maximum adsorption efficiency was calculated as 93.9% and the maximum regeneration efficiency of the adsorbent was found to be 78.8% higher after it had

been washed by alkaline solution of pH 13. The results reflect the feasibility of the nanocomposite as an adsorbent with a potential application in wastewater treatment technologies.

KEYWORDS: Kaolin; SEM; Zeolite A; Cerium Oxide Adsorbent; Methylene Blue; Kinetics

1. INTRODUCTION

Dyes are important coloring agents with application in several industries including printing, textiles, food, plastic etc. The release of toxic-colored wastewater from these industries into natural water bodies has led to harmful effects on humans, oceanic life and photosynthesis through the reduction of solar irradiation [1, 2].

Numerous technologies, including biological degradation which uses fungal decolourization as well as chemical and physical methods such as coagulation, electrochemical techniques and ozonation approaches, have been broadly studied to treat wastewater polluted with dyes [1,2,3]. None of these strategies has however been effective in dye molecules removal from polluted water [1]. This has heightened interest in the search for novel materials and simpler methods for purification of water bodies affected by wastewater from industries that uses dye [3].

One of such techniques capable of removing dyes from polluted waterbodies is the use of nanocomposite materials to adsorb the dye molecules [1]. An ideal adsorbent should have a porous structure, high surface area, good physical, mechanical and chemical stability and high affinity for pollutant molecules [3]. The adsorption of an organic molecule by an adsorbent depends on various parameters such as pH of the solution medium, the structure and concentration of the adsorbate, degree off ionization of the adsorbate, temperature, the ionic

strength of dispersion and the structure and surface charge of the adsorbent. An adsorbent surface with highly ionic character is effective for removing organic molecule of opposite ionic character [4]. Research works have shown that Zeolite; a microporous aluminosilicate material with regular structures consisting of well-defined molecular-sized pores and channels can be engineered to be efficient in removing dye molecules from wastewater. Zeolites frameworks are built by $[SiO4]^{4-}$ and $[AlO4]^{5-}$ tetrahedral, linked together to form cages connected by pore openings of defined size. The presence of $[AlO_4]^-$ in the zeolite framework introduces negative charges which is balanced by cations such as Ca^{2+}, K^+ and Na^+ which are also exchangeable in solution through ionic exchange [5,6]. Several research works have revealed that the nature of their porous framework has a strong effect on its efficiency as an absorbent and as a host material in biomedical and catalytic applications [7].

Dyes are classified as anionic, cationic and nonionic with different molecular sizes [8]. Adsorption of anionic dyes by zeolite has been reported to be low because both zeolite and anionic dyes have similar surface charge characteristic [8,9]. It is also reported that the adsorption capacity of zeolite can be enhanced by modifying the surface with hexamethylenediamine (HMDA), hexadecyltrimethylammonium bromide (HTAB) and cetyltrimethylammonium bromide (CTAB) [9,10,11]. In addition, the charge characteristics of zeolite can be modified to enhance its adsorption of cationic dyes by introducing functional groups or by encapsulation of complexes in the zeolites framework to increase the number of active sites [12,13,14].

Currently, much attention is paid to nanoparticle adsorbents, such as Manganese oxide (MnO_2), Iron (IV) Oxide (Fe_3O_4), Titanium dioxide (TiO_2), $MnFe_2O_4$ and Cerium oxide (CeO_2), due to

their ability to exist in multivalent state and the formation of complexes within host materials. Interestingly, one of the abundant and less costly rare earth metal oxides is Cerium oxide which has been studied as a catalyst providing excellent physical and chemical properties [15]. Among the rare earth metal oxides, Ceria has the lowest solubility in acidic media and does not elute during its use in the removal of harmful ions from aqueous solutions. In addition, cerium is a multivalent element, capable of forming several metal complexes [16]. One interesting property of the CeO_2 nanocrystals is that they exhibit a point zero charge at pH 8.0 implying that they are positively charged under pH less than 8.0 and negatively charged at pH values greater than 8.0 [17]. In many environmental remediation applications, cerium oxide had shown a high adsorption capacity for various anions and cations including fluoride and arsenic which makes it attractive as an adsorbent [18,19]. The authors are hypothesizing that, with tunable surface charge characteristics of zeolite and CeO_2, when developed into a nanocomposite, CeO_2 and zeolite may act synergistically to enhance their capacity to adsorb cationic methylene blue dye from water bodies.

In this work, natural aluminosilicate-based deposit Kaolin have been sampled from Saltpond, in the Central region of Ghana. Zeolite/Cerium oxide nanocomposite (Z/CeO_2-NC) was hydrothermally synthesize. The as-synthesized Zeolite and its nanocomposite (Z/CeO_2–NC) were characterized by X-Ray Diffraction (XRD), Fourier Transform Infra-Red (FT-IR), Energy Dispersive X-Ray Spectroscopy (EDX) and Scanning Electron Microscopy (SEM) to confirm the formation of Zeolite and Cerium Oxide nanoparticles. The adsorption kinetics of methylene dye molecules onto the Z/CeO_2–NC and the thermodynamic Gibb's free energy parameter was studied to understand the adsorption characteristics of the zeolite nanocomposite.

2.0 MATERIALS AND METHODS

2.1. Raw Materials

All the chemicals used in this study were of analytical grade and were used without purification. Sodium hydroxide (NaOH, 99%), Hydrochloric acid (HCl, 99%), Cerium (III) nitrate hexahydrate ($Ce(NO_3)_3$•6H2O, 99.0%), and Methylene blue dye were purchased from Sigma Aldrich (UK). In addition, Kaolin was obtained from Saltpond in the Central region of Ghana.

Methylene blue is a cationic dye made of heterocyclic aromatic chemical compound with the molecular formula of $C_{16}H_{18}N_3SCl$ and molecular weight of 319.85 g/mol. The MB was used as the adsorbate.

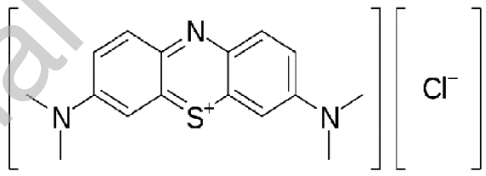

Figure 1. Molecular Structure of Methylene Blue

2.2. Synthesis of Zeolite A

The method used for the synthesis of Zeolite A is similar to the one reported by Nyankson et al. [20]. At the initial stages of the synthesis, the kaolin particles were sized using Retsch-VS1000 mechanical shaker to dimensions ≤ 75 μm. The fine raw kaolin sample was then calcined at a temperature of 600 ℃ for 2 hours to convert it to metakaolin, which is more reactive. This stage

was immediately followed by alkaline treatment with a 2 M NaOH aqueous solution using a Solid-to-Liquid (S/L) ratio of 10 g/50 mL. The mixture was stirred continuously using a magnetic stirrer for 30 min to give a homogeneous mixture and then allowed to age for 24 hours to allow for nucleation of the zeolite phases. After this, the mixture was then placed in an oven at 100 ℃ for 7 hours to allow the growth of the zeolite crystals. The next stage involved filtration of the mixture and the subsequent washing of the residue until the pH of the filtrate was near neutrality. The residue separated was then further dried in an oven at 60 ℃ overnight. The dried sample was then crushed and grinded in a mortar with a pestle and sent for characterization.

2.3. Synthesis of Zeolite/Cerium Oxide Nanocomposites

In the synthesis of the Zeolite/Cerium Oxide Nanocomposites (Z/CeO_2-NCs), two optimal masses; 300 mg and 400 mg masses of the $Ce(NO_3)_3 \cdot 6H_2O$ salt were used based on ion exchange calculation in order to avoid overdose and blocking of the zeolite pores. The Z/CeO_2-NCs prepared with 300 and 400 mg of $Ce(NO_3)_3 \cdot 6H_2O$ were designated as Z-300 mg Ce and Z-400 mg Ce, respectively. The measured masses of salt were each dissolved in water and stirred continuously for 30 minutes to form a homogenous solution. This was immediately followed by the addition of 6 g of the as-synthesized zeolite into each of the aqueous solution and stirred continuously for 20 hours and at 150 rpm under room condition. Each mixture was treated slowly with 50 mL 0.1 M aqueous solution of NaOH under vigorous stirring for 1 hour to allow for precipitation. The precipitate was filtered, washed by centrifuging with deionized water and dried in an oven at **50** ℃ overnight. The final stage involved calcination of the dried nanocomposites at **550** ℃ for 2 hours to allow for the CeO_2 nanoparticles formation.

2.4. Characterization of Nanocomposite

UV-Vis spectroscopy

The process of adsorption of the dye molecules onto Zeolite/Cerium oxide nanocomposite surface was monitored using UV-Vis spectroscopy. A scan between 200 - 900 nm wavelengths using a GENESYS 10S UV-Vis (version v4.005 2L5S048209) was carried out. The maximum adsorption peak for MB was observed at 665 nm wavelength and the corresponding absorbance measured were used to extract concentration values from a calibration curve.

X-Ray Diffraction (XRD)

Powder XRD patterns were recorded using the Empyrean PANalytical series 2 X-ray Diffractometer (XRD) with CuKα (1.54Å) radiation source and a tube operating at 40 mA and 40 kV. The phases in the samples were identified using X'Pert Highscore plus database software.

Fourier Transform Infra-Red (FTIR) Spectroscopy

In this work Attenuated Total Reflectance (ATR) was employed with single bounce diamond anvil ATR accessory fitted to a Thermo-Fisher Nicolet IS50 FT-IR spectrometer.

Scanning Electron Microscopy (SEM) and Energy Dispersive X-Ray Analysis (EDX)

The structural morphology and empirical elemental compositions were estimated using energy dispersive X-ray spectroscopy (EDX)-Zeiss EVO LS10 scanning electron microscopy (SEM) equipped with Oxford INCA X-act detector.

2.5. Adsorption Experiments and Kinetics

The aim of the present study is to investigate the ability of the Z/CeO_2-NCs adsorbent to remove MB dye molecules from solution as well as describe the adsorption mechanisms using kinetic and isotherm models.

A series of experiments were conducted before the optimal adsorbent loading of 2.8 mg Z/CeO_2-NC in 3.5 mL MB solution was arrived at [20]. All adsorption experiment was performed in a batch sequence using adsorbent loading of 2.8 mg, adsorbate pH of 9 and at a temperature of 25 °C. In the batch adsorption experiments, 2.8 mg of the Z/CeO_2-NCs was placed into a cuvette followed by the addition of 3.5 mL of MB solution (2 mg/L). The cuvette with the mixture was

then placed in the Genesys 10S UV–Vis spectrophotometer and a set of absorbance data taken over a period of 3 hours at the MB characteristic monochromatic wavelength (λ_{max}) of 665 nm.

pH is a parameter capable of having effect on the adsorption and desorption process in a batch adsorption study through altering the charge surface characteristics an adsorbent [21]. Desorption of MB molecules from an adsorbent in an alkaline medium is as a result of the excess OH^- reacting with the cationic sites of the MB molecules in solution [22,23].

From the adsorption experiments, the adsorption capacity, q_t (mg/g) which represents the amount of dye adsorbed per unit weight of zeolite, mg/g and the dye removal efficiency was then calculated using the equation as shown below:

$$\text{Adsorption Capacity, } q_t = \frac{(C_o - C_t)}{W} V \quad (1)$$

$$\text{Removal Efficiency (\%), } R = \frac{(C_o - C_t)}{C_t} X\ 100 \quad (2)$$

Where,

C_o - The Dye concentration at time, t=0 (mg/L)

C_t - The Dye concentration at time, t=t (mg/L)

V - The volume of MB solution (mL)

W - The mass of the Z/CeO_2-NCs adsorbent used (mg)

After this a regeneration study was carried out in order to investigate the removal efficiency of the spent adsorbent after washing it with an aqueous solution of varying pH values of 3, 5, 7, 9, 11 and 13 using 0.1 mol/L NaOH and HCl solutions.

Adsorption Kinetics

The purpose of carrying out an adsorption kinetic study is to describe the solute uptake rate from the solute-solution interface. The Pseudo-First-Order (PFO) Lagergren equation, Pseudo-Second-Order (PSO) rate equation and the intra-particle diffusion model are among the common models for investigating the mechanism for dye molecule uptake by adsorbents [24]. In this work, the PFO kinetic, PSO kinetic and an Intra-particle diffusion models were all employed.

The PFO kinetic model by Lagergren states that the solute uptake rate is directly proportional to the difference in concentration of the solute and the equilibrium saturation concentration on the adsorbent [24]. Thus,

$$\frac{dq_t}{dt} = k_1(q_e - q_t) \quad (3)$$

Where;

q_t – Amount of dye adsorbed at time "t" in minutes (mg/g)

q_e – The equilibrium dye adsorption capacity (mg/g)

k_1 – The rate constant of PFO (min^{-1})

Integrating Eq. (3) above with boundary conditions; q_t = 0 at t = 0 and $q_t = q_t$ at t = t and rearranging gives a linear form of the kinetic equation as shown in Eq. 4;

$$\log(q_e - q_t) = \log q_e - \frac{k_1}{2.303}t \quad (4)$$

The PSO kinetic model (Eq. 5) proposed by Ho and McKay states that the rate of solute uptake is directly proportional to the square of the difference in concentration of the solute and the equilibrium saturation concentration on the adsorbent [25].

Thus;

$$\frac{dq_t}{dt} = k_2(q_e - q_t)^2 \quad (5)$$

Where;

q_t – Amount of dye adsorbed at time "t" in minutes (mg/g)

q_e – The equilibrium dye adsorption capacity (mg/g)

k_2 – The rate constant of PSO (g mg^{-1} min^{-1})

Integrating Eq. (5) above with initial conditions; q_t = 0 at t = 0 and $q_t = q_t$ at t = t and rearranging gives a linear form of the kinetic equation as shown below;

$$\frac{t}{q_t} = \frac{1}{k_2 {q_e}^2} + \frac{t}{q_e} \quad (6)$$

A linear graph of $\frac{t}{q_t}$ against t is plotted and the value of q_e *and* k_2 **(**The rate constant of pseudo-second order**)** were deduced.

The third model, intra-particle diffusion model (Eq. 7), was proposed by Weber and Morris in 1962 has been widely applied for the analysis of adsorption kinetics to determine the rate-controlling steps. The intra-particle diffusion is controlled by film diffusion, pore diffusion or surface diffusion or a combination during the adsorption phenomenon on the pore surface [26]. The model is described as;

$$q_t = k_i t^{0.5} + C_i \quad (7)$$

Where;

C_i – The intercept which corresponds to the boundary layer thickness (mg/g)

k_i – Intra-particle diffusion rate constant (mg/g•$min^{-0.5}$)

C_i and k_i can be directly determined from the liner plot of q_t against $t^{0.5}$ as the slope and intercept respectively. The larger is the value of C_i, the greater is the boundary layer effect.

Sorption Isotherm Models

Two different isotherm models; Langmuir and Freundlich Isotherms are used to describe the equilibrium adsorption data and to understand the extent of favorability of the adsorption. The applicability of the isotherm equation to the adsorption study done was compared by analyzing the correlation coefficients [27].

The Langmuir isotherm is a useful isotherm that assumes that adsorption takes place at specific homogeneous sites within the adsorbent, with a process of homogeneous monolayer adsorption of adsorbate on the surface of the adsorbent [28]. It also assumes that one active site is responsible for adsorbing a dye molecule, and once it is occupied, no additional adsorption can occur at that site. The saturated monolayer isotherm model can be expressed as;

$$Q_e = \frac{Q_m K_L C_e}{1 + K_L C_e} \quad (8)$$

The linearized form of becomes:

$$\frac{C_e}{q_e} = \frac{1}{Q_m K_L} + \frac{C_e}{Q_m} \quad (9)$$

Where:

Q_m – The maximum adsorption capacity at monolayer (mg/g)

K_L – The Langmuir adsorption constant (L/mg)

C_e – The equilibrium concentration of the adsorbate

The values of Q_m and K_L can be determined from the linear plot of C_e/q_e versus C_e.

It is well known that the separation factor (R_L) is crucial in determining the suitability of Langmuir isotherm to model the adsorption process. A value of $0 < R_L < 1$ indicates that it is a favorable adsorption process, while $R_L > 1$ shows that it is an unfavorable adsorption process,

R_L = 1 means linear adsorption, and R_L = 0 signifies irreversible adsorption. R_L can be estimated mathematically from Eq. (10)

$$R_L = \frac{1}{1+K_L C_o} \quad (10)$$

Where:

R_L - The separation factor (dimensionless),

K_L - The Langmuir adsorption constant (L/mg)

C_o -The initial concentrations of adsorbate (mg/L).

On the other hand, the Freundlich isotherm describes a heterogeneous multilayer adsorption system with interactions between adsorbed molecules. The Freundlich isotherm is an empirical equation that is derived by assuming a heterogeneous surface with a non-uniform distribution of heat over the surface of adsorbent [29] and it can be represented by

$$Q_e = K_F C_e^{\frac{1}{n_f}} \quad (11)$$

The linearized form of the Eq. (11) is:

$$\ln Q_e = \ln K_F + \frac{1}{n_f} \ln C_e \quad (12)$$

Where;

Q_e- The adsorption capacity at equilibrium (mg/g)

C_e- The liquid phase concentration of adsorbate at equilibrium (mg/L)

K_F - The Freundlich constant (mg/g)

n_f - The heterogeneity factor.

$1/n_f$ relates to adsorption intensity. The values of n_f in the range of 1 to 10 represent favorable adsorption. A smaller value of $1/n_f$ below unity indicates a stronger bond between adsorbate and adsorbent.

3.0 RESULTS AND DISCUSSIONS

3.1. X-Ray Diffraction (XRD)

XRD analyses were done on the as-synthesized pure zeolite (Z) and Z/CeO_2-NCs in order to identify the phases present as shown in Figure 2.

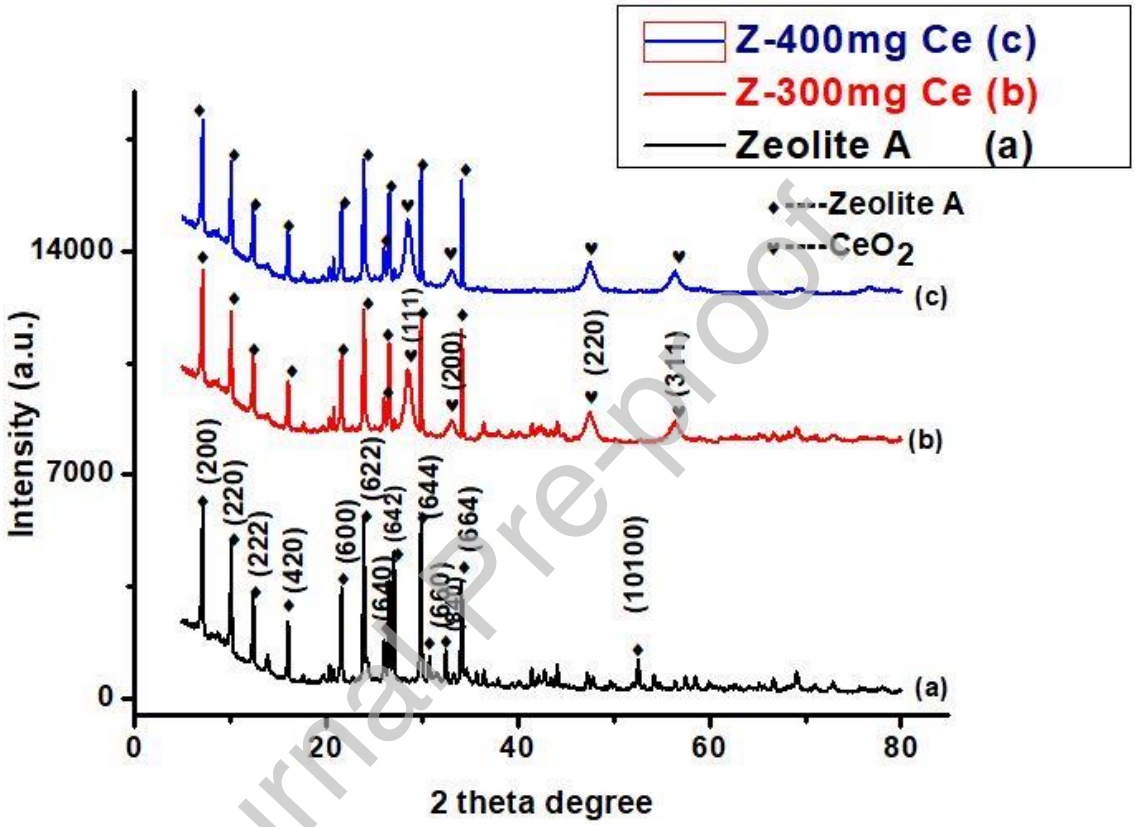

Figure 2. XRD of (a) Pure Zeolite (Z) (b) Z/300 mg Ce (c) Z/400 mg Ce

The diffraction pattern of the as-synthesized zeolite was matched with that of literature and identified as Zeolite Linda Type A. Also, the zeolite composite recorded major zeolite peaks at 2θ peak positions of; 7.15°, 10.14°, 12.42°, 16.08°, 21.64°, 23.96°, 26.08°, 26.62°, 27.09°, 29.92°, 34.16° and 52.56° and these corresponds to the (200), (220), (222), (420), (600), (622), (640), (642), (644), (660), (840) and (664) planes respectively which confirm that the as-

synthesized zeolite was of type Linda Type A with a chemical formula $Na_{96}Al_{96}Si_{96}O_{384}$ ·216 H_2O [30].

Again, the intense XRD diffraction peaks for Figure 2 (b) and (c) located at angles (2θ) = 28.54°, 33.12°, 47.49° and 56.33° respectively corresponded to the (111), (200), (220) and (311) planes of Cerium Oxide nanoparticles (CeO_2) as reported by Arumugam et al. [31]. Using the Scherer's equation (Eq. (13)), the crystallite size of the pure zeolite and the composites were deduced at an intense 2 theta peak position of 29.9°, wavelength, λ = 0.154 nm and a shape factor, K = 0.94. This calculation helped to analyze the effect of the variation in the composition on the crystallite size of the as-synthesized zeolite composite. The Scherer's equation is given below;

$$L = \frac{0.94\lambda}{\beta cos\theta} \quad (13)$$

Where:

λ = wavelength of X-Ray (Cu Kα),

β= Full width at Half Maximum,

θ = Bragg's Angle,

L = crystallite size

From the results, it was observed that the crystallite size of Pure Zeolite was 57.4 nm and that of Z/300 mg Ce and Z/400 mg Ce were 28.7 nm and 24.8 nm respectively. By comparing these three, it can be observed that the compositional variation led to a decreased crystallite size. Also, by comparing the two composites, it was further observed that the one with the higher

composition of $Ce(NO_3)_3 \cdot 6H_2O$ salt had the smallest crystallite size. The smaller the crystallite size, the larger the surface area of the adsorbent exposed to the dye molecules and hence the better dye removal efficiency.

3.2. Energy Dispersive X-Ray Analysis (EDX)

The EDX shows the elemental composition present in a given sample. The EDX analysis of the composite detected aluminum, oxygen and silicon which indicates the presence of zeolite which is an aluminosilicate. The detection of cerium confirms the presence of the cerium oxide phase in the zeolite/ cerium oxide nanocomposite. The EDX results is summarized in Figure 3.

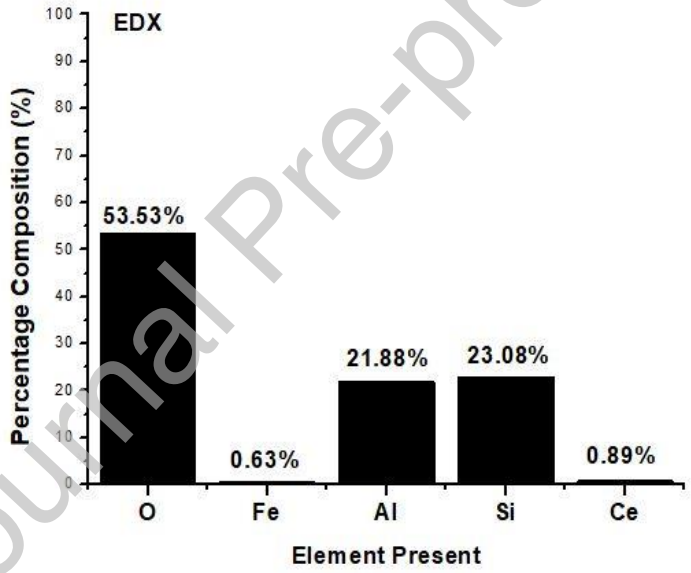

Figure 3. EDX showing the elemental composition present in the Zeolite/Cerium Oxide nanocomposite.

3.3. Fourier Transform Infra-Red (FTIR) Analysis

FTIR spectroscopy is used to identify the IR spectra corresponding to the functional groups and the vibrational bands present in both the pure zeolite and Z/CeO_2-NCs in the spectral range of 4000-400 cm^{-1}, as shown in Figure 4.

The spectral of pure zeolite as shown in Figure 4(a) exhibits intense peaks at 546, 663, 974, 1645 and 3339 cm^{-1}frequencies while that of the Z/CeO_2-NCs exhibited intense peaks at 457, 548, 663, 984, 1653 and 3351 cm^{-1} for sample Z/300 mg Ce and 457, 551, 663, 995, 1653, and 3350 cm^{-1} for sample Z/400 mg Ce as shown in Figure 4(b and c).

The IR spectra located at position A (457cm^{-1}) corresponds to the Ce-O stretching which was close to 450 cm^{-1} as reported by Goharshadi et al [32]. Also, the band at position C (547, 548 and 551 cm^{-1}), found within the band range of 650-500 cm^{-1} represent the external T-O linkage (T = Si or Al) due to the presence of a double ring in the zeolite framework. The spectral at D (663 cm^{-1}) found between 720-650 cm^{-1} indicate internal vibrations due to symmetric stretching of Si-O-Si silica framework in the formed zeolite. The frequencies at position E (975,984 and 995 cm^{-1}) represent the internal vibrations due to asymmetric stretching of Si–O–Al tetrahedral.

The weak band at position F (1645, 1653, 1653 cm^{-1}) arises from the bending mode of water molecules**.** All these characteristic observations confirm the formation of zeolite. Finally, the band at present at position G (3339, 3351 and 3470 cm^{-1}) is attributed to the stretching vibrations of O-H group.

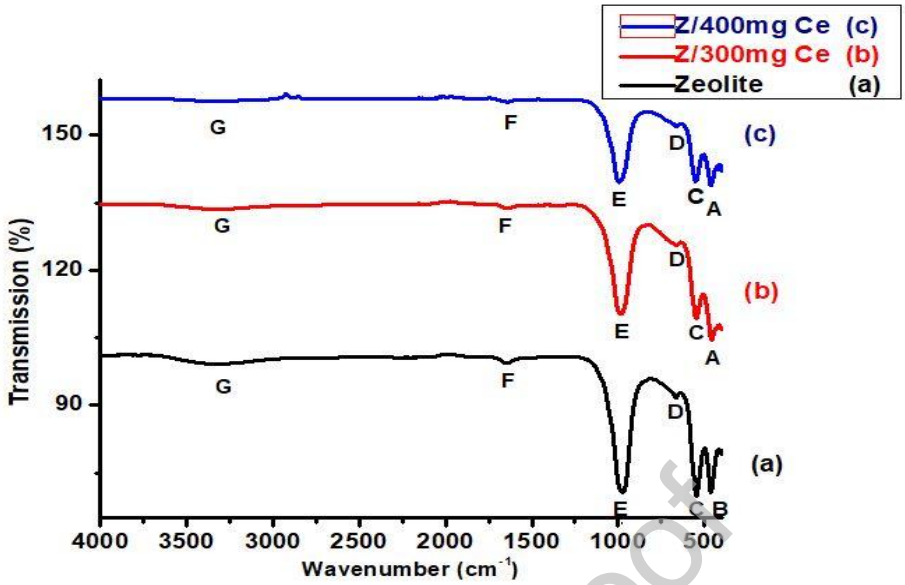

Figure 4. FTIR spectra of (a) Pure Zeolite (Z) and (b), (c) Zeolite/Cerium Oxide nanocomposite for sample Z/300 mg Ce and Z/400 mg Ce respectively.

The shift in the characteristic peaks by 5-10 cm^{-1} is as a result of the CeO_2 incorporation [33]. That means that $Ce(NO_3)_3 \cdot 6H_2O$ salt addition has some influence on the zeolite framework. From the analyses of the data, it is observed that the IR spectra confirmed the evidence of the formation of zeolite and Cerium Oxide phases.

3.4 Scanning Electron Microscopy (SEM) Analysis

The SEM gives information on the morphological structure of synthesized zeolite and the zeolite/cerium oxide nanocomposite. Mohammadi & Pak (2002) reported that zeolite A is cubic structured. From Figure 5 (a) the formation of cubic zeolite A structures can be observed [34]. By comparing the two diagrams (Figure 5 (a and b)) it can be deduced that the presence of the spherical structure interspersed within the morphology of the composite can be attributed to the formation of cerium oxide phases [31, 35].

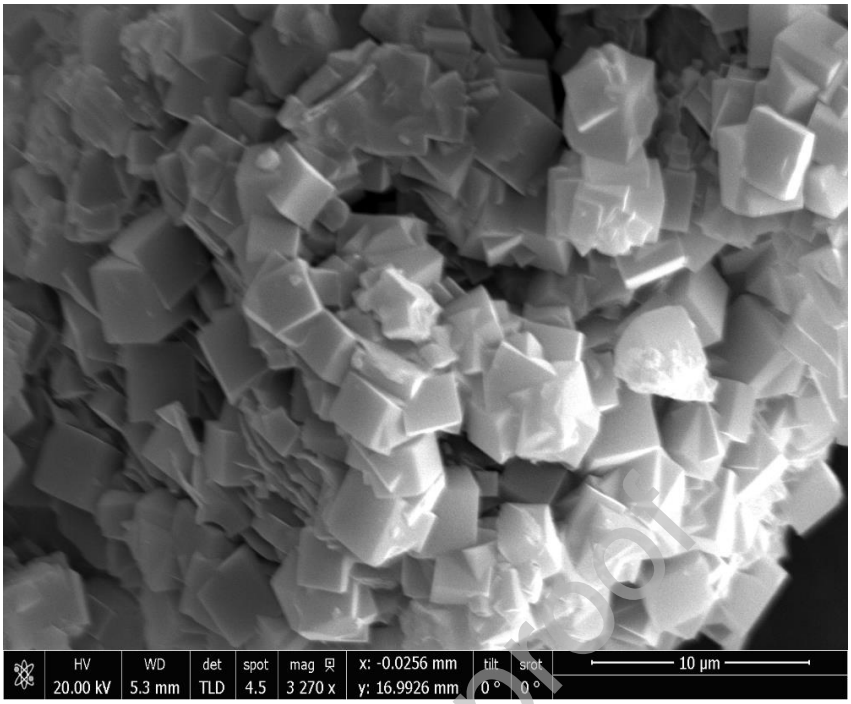

Figure 5. (a) SEM of Pure Zeolite A

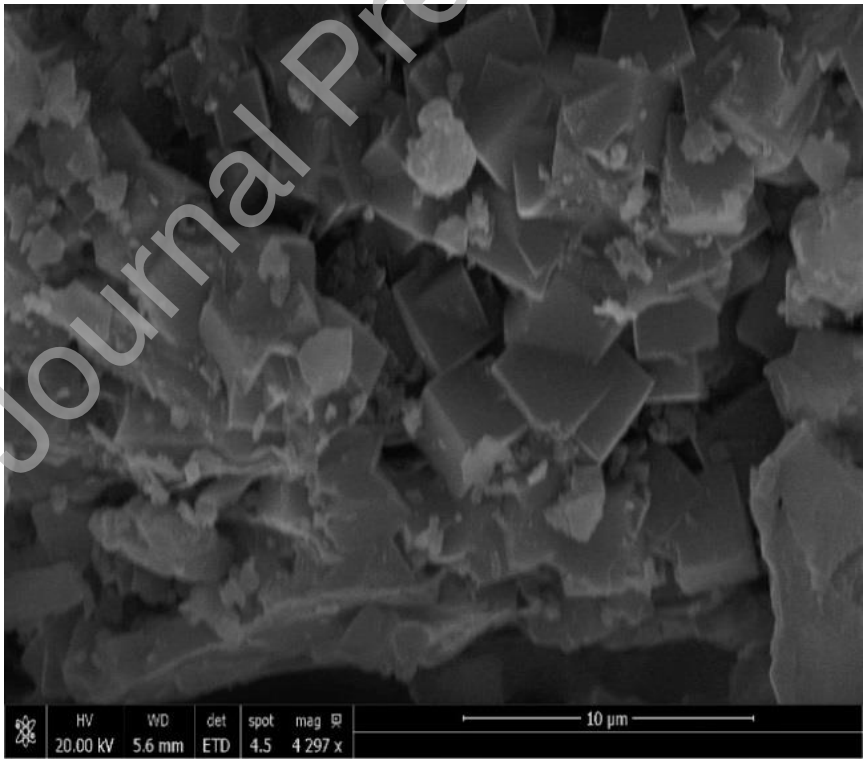

Figure 5. (b) SEM of Zeolite/Cerium Oxide nanocomposite

3.5. Equilibrium Curve

The capacity of Z/CeO_2-NCs to adsorb MB dye molecules from solution was examined and compared to that of the pure zeolite as shown in Figure 6. Overall it was observed that the concentration of the MB dye decreased with time and the amount of dye uptake, q_t (mg/g), increased with contact time. The graph depicts that the dye uptake occured in two phases with a first rapid initial phase of adsorption within the first 10 minutes followed by a gradual second phase attaining saturation after 3 hours, which all contributed to the total adsorption process. The rapid initial stage of adsorption was an instantaneous surface adsorption resulting from the presence of vacant adsorption site as well as the presence of high concentration gradient. The adsorption by pure zeolite can be attributed to the negative surface charge of the zeolite leading to a high electrostatic attraction between the negatively charged zeolite and the positively charged cationic MB [36]. It has been reported that pHzpc of zeolite is 7.8. Below pH 7.8 the surface of zeolite is positively charged and above 7.8 the zeolite surface is negatively charged. The pH of the methylene blue dye used for the study was 9. Hence the zeolite possessed a negatively charged surface at pH of 9 resulting in a high electrostatic adsorption of the cationic MB molecules from solution [37].

After 3 hours of adsorption, Z/CeO_2-NCs exhibited a higher dye removal efficiency as compared to that of the pure zeolite. The higher efficiency of the Z/CeO_2-NCs to adsorb MB dye molecules from solution is attributed to the presence of Cerium Oxide nanoparticles. Pelletier et al. reported that CeO_2 nanocrystals exhibits a point zero charge at pH 8.0 implying that they are positively charged at pH less than 8.0 and negatively charged at pH values greater than 8.0 [17]. Since the adsorbate media (MB) used for this study had a pH of 9, the CeO_2 nanoparticles possessed a negatively charged surface. The negatively charged CeO_2 provided additional adsorption sites

that enhanced the adsorption of cationic dye MB from solution. The adsorption therefore occurred as a result of the electrostatic interaction between the positively charged cationic MB and the negatively charged CeO_2 and zeolite. The results from the adsorption studies are summarized in Table 1. As can be seen in the Table 1, the adsorption efficiency of Z/400mb Ce was higher than that of Z/300 mg Ce. The relatively higher efficiency of the Z/400 mg Ce was due to the increase in cerium oxide content than that of Z/300 mg Ce with a lower amount of cerium oxide content. More adsorption sites were therefore available in the sample with higher amount of CeO_2. Pure zeolite attained the least efficiency in the removal of the MB dye.

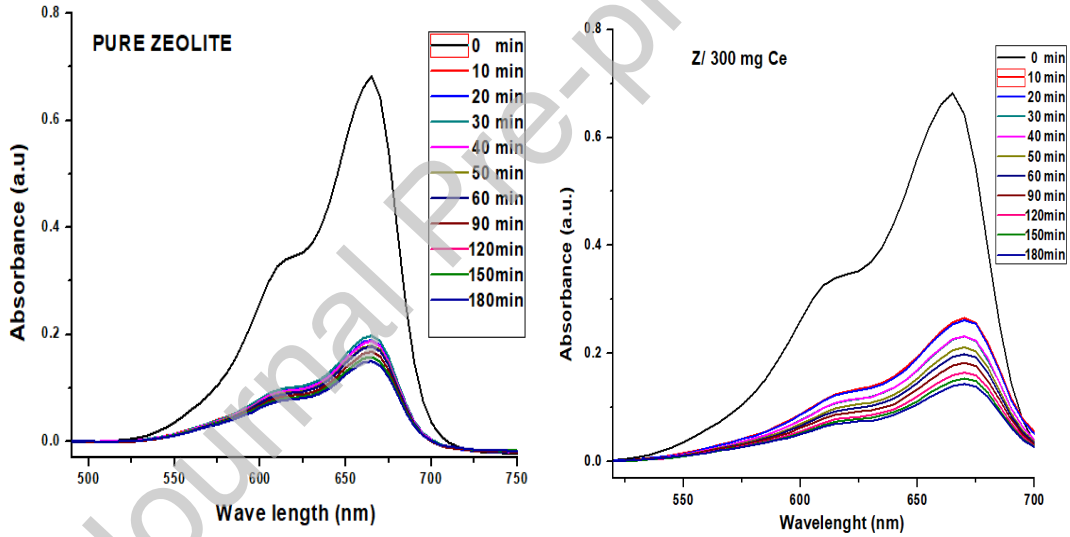

(a) (b)

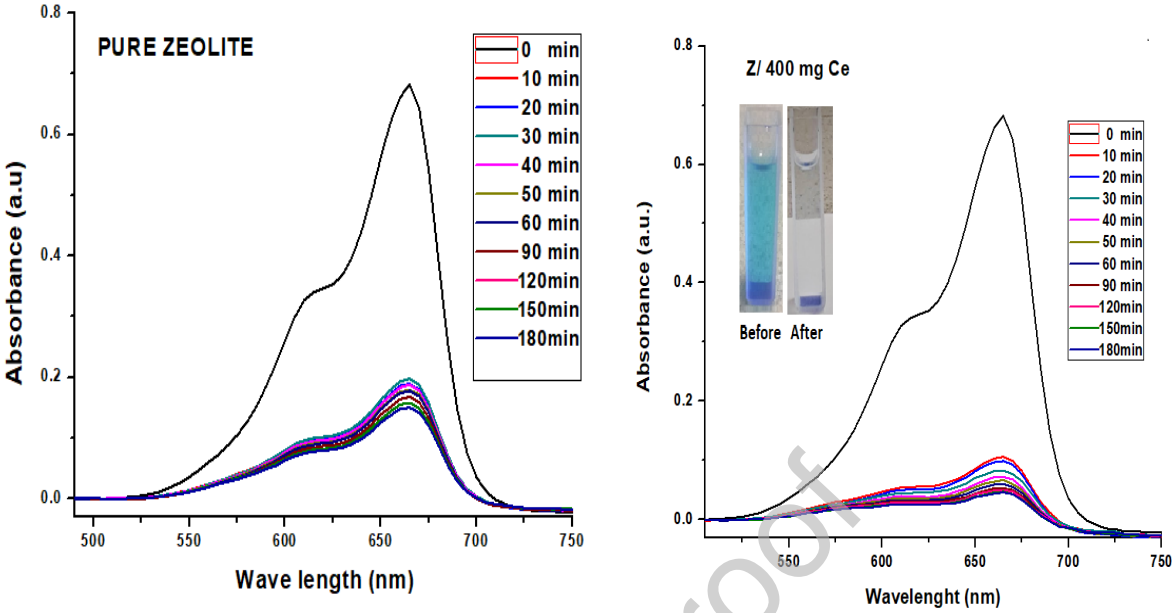

(a) (c)

Figure 6. Absorbance intensity level at various time interval for (a) Pure Zeolite (b) Z/300 mg Ce and (c) Z/400 mg Ce

Table 1. Shows the removal efficiency of pure zeolite, Z/300 mg Ce and Z/400 mg Ce

Sample	Initial Absorbance	Absorbance after 3 h	Removal Efficiency (%)
Pure Zeolite	0.740 ± 0.06	0.145 ± 0.005	80.4 ± 0.7
Z/300 mg Ce	0.739 ± 0.04	0.139 ± 0.007	81.1 ± 0.9
Z/400 mg Ce	0.740 ± 0.09	0.045 ± 0.005	93.9 ± 0.7

3.6. Effect of Contact Time and Initial Dye Concentration

Equilibrium experiments were conducted by contacting 2.8 mg of adsorbent in 3.5 mL of the adsorbate at different initial concentrations (2-10 mg/l) of pH 9 and at 25 ^{O}C. The effect of

contact time was also examined. The results for the effect of contact time and initial dye concentration are presented in Figure 7. It was observed that the amount of MB adsorbed onto the adsoebent increaesd with incresae in MB concentration. Also, the amount of MB adsorbed increased with contact time and its adsorption capacity for MB at equilibrium was increased from 0.60 to 1.07 mg/g and 0.76 to1.32 mg/g for sample Z/300 mg Ce and Z/400 mg Ce, respectively. This observation is as a result of the increase in the driving force (concentration gradient) with increase in initial dye concentration. The increased concentration gradient increased the transfer of MB from the solution medium onto the surface of the nanocomposite [36-38].

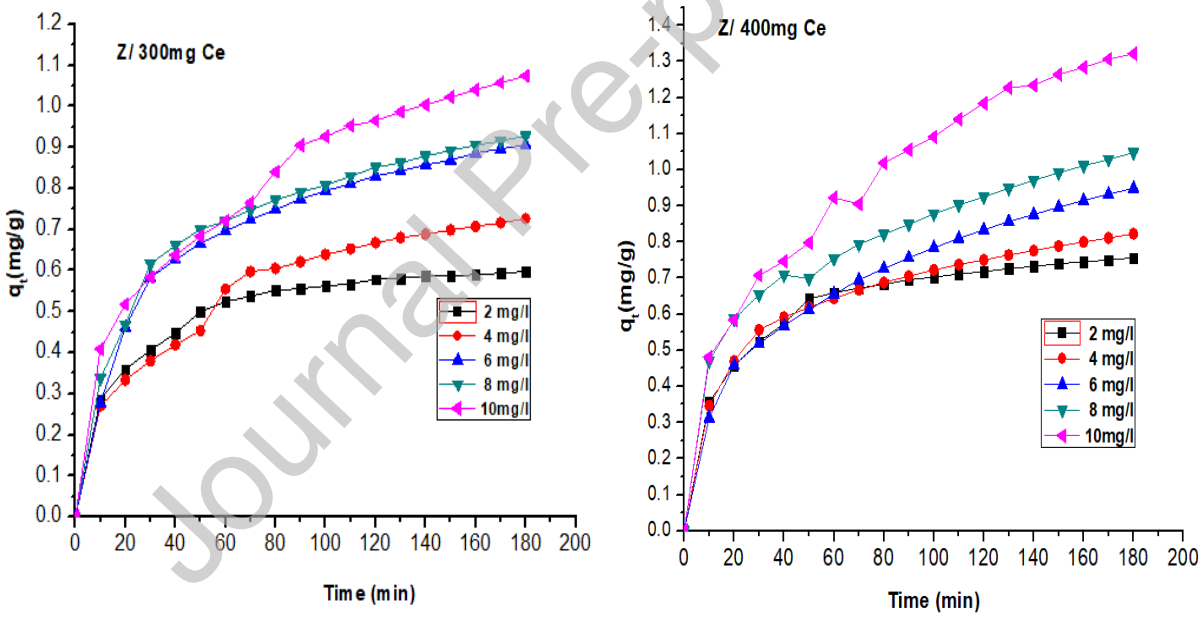

(a) (b)

Figure 7. Effect of contact time on initial dye concentration onto (a) Z/300 mg Ce and (b) Z/400 mg Ce

3.7. Kinetic and Equilibrium Sorption Isotherm Models

Kinetic Models

The pseudo first order (PFO), pseudo second order (PSO) and intra-particle models were used to describe the adsorption kinetics of the MB dye onto the adsorbent surfaces. The fitting of the adsorption data unto the models are shown in Figure 8 (a, b and c). The best-fit model was selected based on the linear regression correlation coefficient, R^2, values. From the study, it was observed that the R^2 values of the PSO models (0.99276 and 0.99789) were greater than that of the PFO models (0.44513 and 0.43577) for Z/300 mg Ce and Z/400 mg Ce, respectively. This implied that the adsorption mechanisms of the adsorbate unto the zeolite nanocomposite adsorbent were controlled by the PSO. A PSO adsorption means that the overall rate of MB adsorption is controlled by a chemical process through the sharing of electrons or by covalent forces through the exchange of electrons between the adsorbent and adsorbate [25]. This confirms that, the adsorption process was controlled by the electrostatic interaction between the negatively charged surface of zeolite and CeO_2, and the positively charged cationic MB. Also, by comparing the two graphs Figure 8 (a and b), it can be observed that Z/400 mg Ce had a higher adsorption rate than Z/300 mg Ce indicating that the amount of CeO_2 nanoparticle present in a composite plays a major role in the adsorption process. The higher the amount of CeO_2 nanoparticles in the nanocomposite, the faster the rate of adsorption.

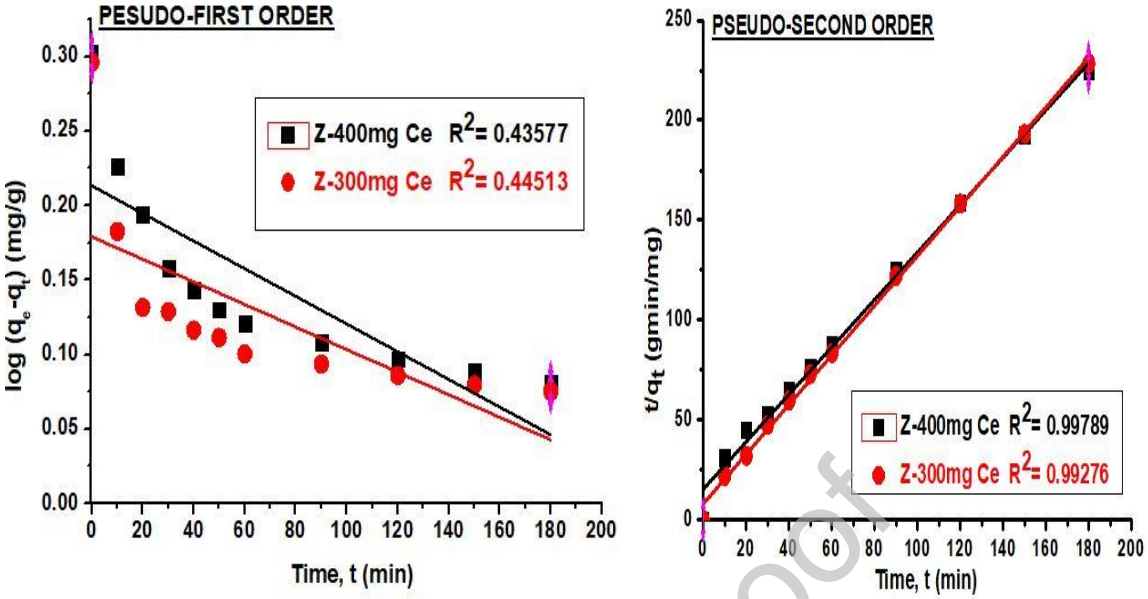

(a)

(b)

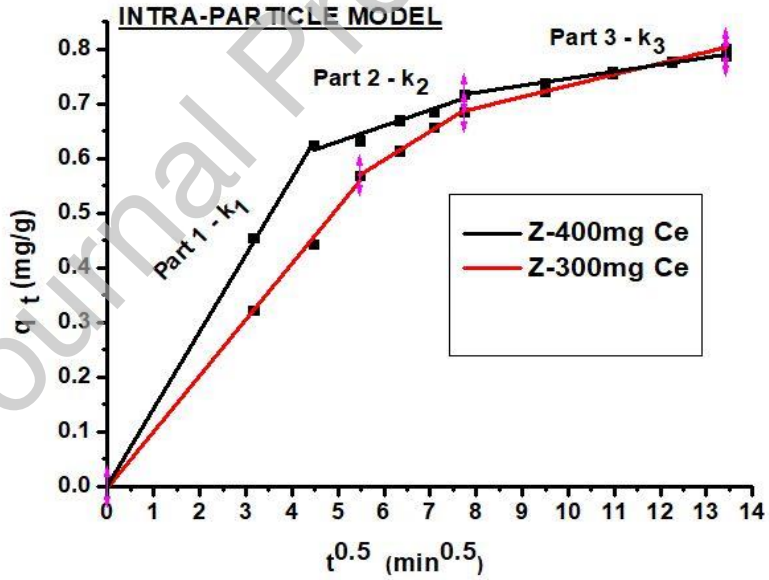

(c)

Figure 8. Models describing the adsorption process. (a)Pseudo-first Order (b) Pseudo-second order and (c) Intra-Particle model

The intra-particle model describes the rate-controlling steps of adsorption process in three stages based on weber-Morris equation. The first stage (part 1) with steeper slopes k_1(0.10233 and 0.14032) for Z/300 mg Ce and Z/400 mg Ce, respectively represents a faster adsorption process due to the electrostatic interaction between the adsorbate and the adsorbent. The second stage (part 2) with slopes k_2(0.05229 and 0.02903) represents a more gradual diffusion process indicating that more of the active sites and pores are being occupied by the dye molecule thereby leaving smaller number of active sites for effective adsorption. At stage 3 (part 3), the slopes k_3 (0.02049 and 0.01281) for Z/300 mg Ce and for Z/400 mg Ce, respectively are the least and these indicate that the adsorption process is nearing or at equilibrium as a result of the active sites currently being occupied with dye molecules indicating that there is virtually no further adsorption taking place. The data for the kinetic studies is tabulated in Table 2 below.

Table 2. Summary of data fitted onto various kinetic models

MODELS	Z/300 mg Ce	Z/400 mg Ce
Pseudo-First-Order Kinetic Model		
R^2	0.44513	0.43577
K_1 (min^{-1})	0.00076 ± 0.00002	0.00093 ± 0.00005
Pseudo-Second-Order Kinetic Model		
R^2	0.99276	0.99789
K_2 (g min/mg)	1.14655 ± 0.03126	1.22038 ± 0.01936
Q_e (mg/L)	1.97 ± 0.08	2.01± 0.05
Intra-Particle Diffusion Model		
K_1 ($min^{0.5}$ g mg^{-1})	0.10233 ± 0.00342	0.14032 ± 0.00691
K_2 ($min^{0.5}$ g mg^{-1})	0.05229 ± 0.00149	0.02903 ± 0.00095

K_3 ($min^{0.5}$ g mg^{-1})	0.02049 ± 0.00387	0.01281 ± 0.00033

Sorption Equilibrium Isotherm Models

Langmuir and Freundlich isotherms (Figure 9) were used to describe the adsorption mechanisms for the interaction of dye molecules on the adsorbent surface and to determine the adsorption capacity. The related correlation coefficients (R^2) and other constant values are given as shown in Table 3. The Langmuir equation fitted the adsorption process very well with a higher R^2 value of 0.99264 and 0.99778 as compared to the Freundlich isotherm with relatively lower R^2 values of 0.80596 and 0.88472 for Z/300 mg Ce and Z/400 mg Ce, respectively. The Langmuir isotherm model indicates that adsorption sites of the nanocomposite are equally alike and energetically charged thereby providing a homogeneous monolayer surface coverage of MB molecules on surface of the Z/CeO_2-NCs which has an identical adsorption activity and only one dye molecule can be adsorbed on each adsorption site [37]. In addition, it was observed that the maximum adsorption capacity (Q_m**)** of the nanocomposites increased with increased CeO_2 nanoparticles content with Z/300 mg Ce and Z/400 mg Ce having Q_m values as 2.02 and 2.51 mg/g, respectively, indicating the monolayer saturation at equilibrium due to the monolayer coverage on the adsorbent by the MB dye molecules. The Langmuir constant K_L was higher in Z/400 mg Ce indicating a higher affinity binding of MB molecule onto the adsorbent. The separation factor R_L which lied within the range $0 < R_L < 1$ confirmed the favourability of adsorption of MB by the nano-adsorbent [28].

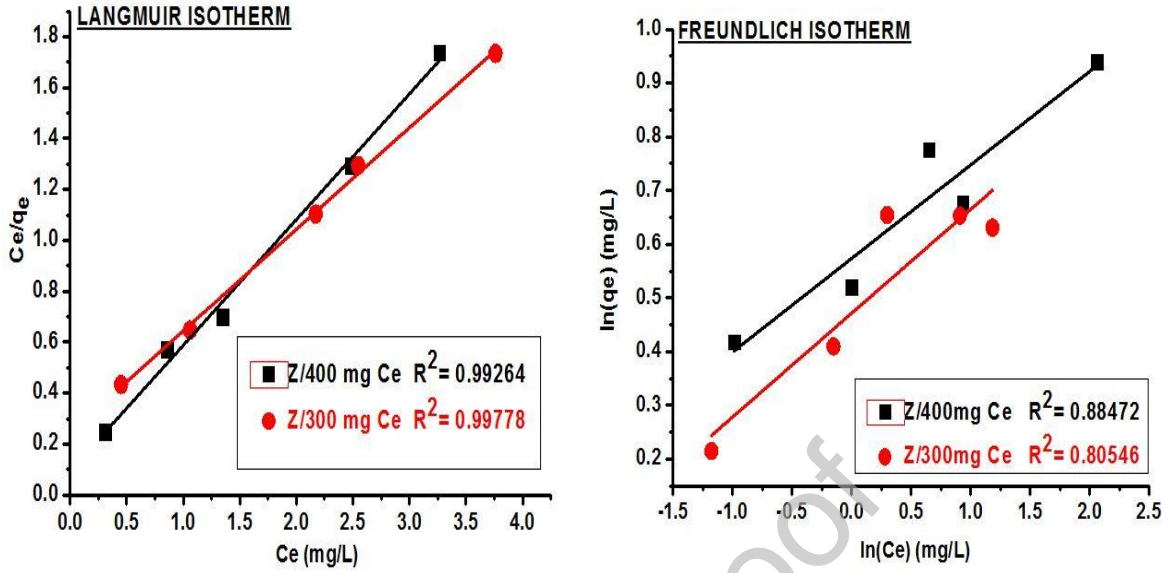

(a) (b)

Figure 9. (a) Langmuir and (b) Freundlich Isotherm plot for sample Z/300 mg Ce and Z/400 mg Ce

Table 3. Summary of data fitted on the isotherm model

SAMPLE	LANGMUIR ISOTHERM				FREUNDLICH ISOTHERM		
	Q (mg/g)	R^2	K_L	R_L	n	R^2	K_F
Z/300 mg Ce	2.02 ± 0.03	0.99264	1.6285 ± 0.00657	0.06 ± 0.01-0.23 ± 0.02	5.1746 ± 0.4218	0.80596	1.6021 ± 0.0892
Z/400 mg Ce	2.51 ± 0.07	0.99778	5.2706 ± 0.00981	0.02 ± 0.001-0.09 ±0,001	5.7435 ± 0.3870	0.88472	1.7742 ± 0.0538

3.8. Gibbs Free Energy Thermodynamic Adsorption Parameter

To estimate the effect of the 25 ^{O}C (298 K) temperature on the adsorption of MB onto the Z/CeO_2-NCs, the change in the Gibb's free energy (ΔG) was calculated using the Eq (14).

$$\Delta G^o = -RTlnK \quad (14)$$

Where ΔG^{O} is the standard Gibb's free energy change (J/mol), R is the universal gas constant (8.314 J/mol K), T is the absolute temperature (K), and K_L is the Langmuir adsorption equilibrium constant (L/mol) [39].

The standard Gibb's free energy was calculated to be -1.208 and – 4.118 KJ/mol for Z/300 mg Ce and for Z/400 mg Ce, respectively indicating that the adsorption process was spontaneous [39].

3.9. Regeneration Capacity

Reusability of adsorbents is a subject of great relevance in the economic development for adsorption processes. The zeolite nanocomposite adsorbents after full adsorption were washed with different pH of 3, 5, 7, 9, 11 and 13 in order to regenerate the adsorbent for reuse. pH is a parameter capable of having effect on the adsorption and desorption process in a batch adsorption study through altering the charge surface characteristics of the adsorbent [21]. The regenerated adsorbents were utilized again for dye adsorption as shown in Figure 10 (a and b). It was observed that adsorbent washed with alkaline medium achieved a higher adsorption rather than those washed with acidic medium. Desorption of MB molecules from an adsorbent in an alkaline medium resulted from the excess OH^- reacting with the cationic sites of the MB molecules in solution [22,23]. Excess H^+ ions were not able to desorb the cationic MB to free the adsorptive sites leading to decrease in dye uptake due to the electrostatic repulsion of both cations. Also, it was observed that the used Z/400 mg Ce showed relatively high regeneration efficiency of about 78.8% as against a regeneration efficiency of 67.0% for Z/300 mg Ce. In both cases, it was realized that the pH at which maximum and minimum efficiency occurred was pH of 13 and 3, respectively. The results from the regeneration studies are summarized in Table 4.

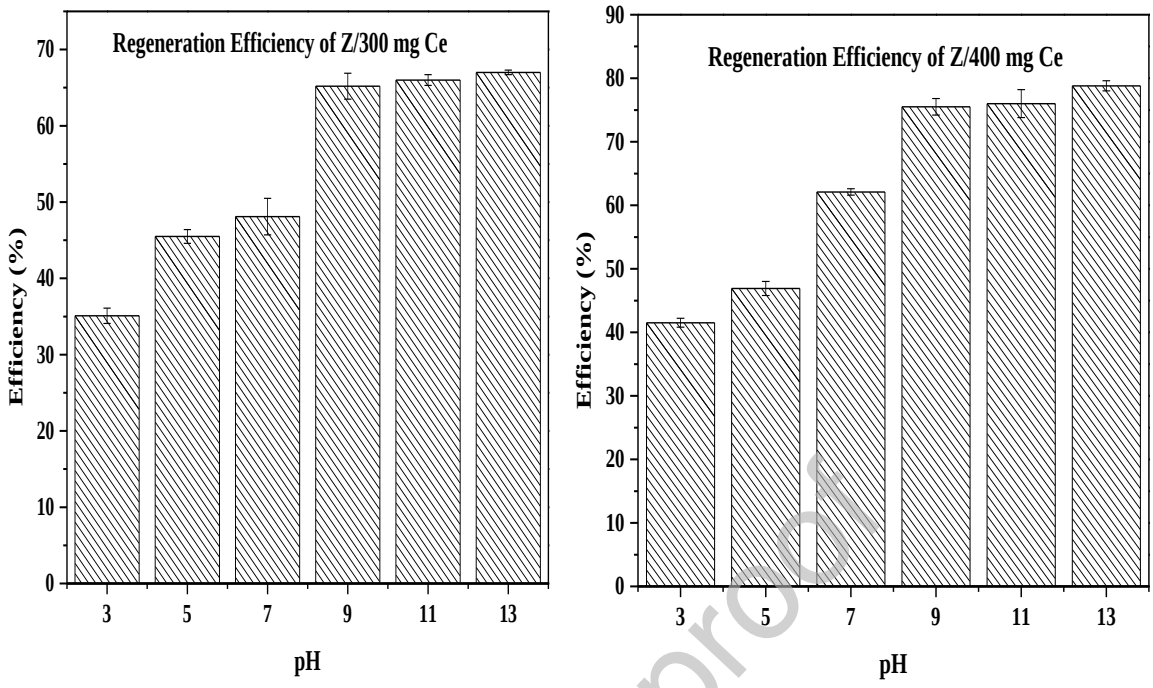

(a) (b)

Figure 10. Regeneration capacity of (a) Z/300 mg Ce and Z/400 mg Ce with various pH

Table 4. Regeneration Efficiency of the zeolite nanocomposites

pH	% Efficiency (Z/300 mg Ce)	% Efficiency (Z/400 mg Ce)
3	35.1 ± 1.0	41.5 ± 0.7
5	45.5 ± 0.9	46.9 ± 1.1
7	48.1 ± 2.4	62.1 ± 0.5
9	65.2 ± 1.7	75.5 ± 1.3
11	66.0 ± 0.7	76.0 ± 2.2
13	67.0 ± 0.3	78.8 ± 0.8

4. CONCLUSION

The potential of Zeolite/ CeO_2 nanocomposite as a dye removal adsorbent has been successfully explored. From the experiment, it was observed that the adsorption of the MB dye molecules unto the Zeolite/ CeO_2 nanocomposite adsorbent (Z/CeO_2-NCs) was controlled by the Pseudo Second Order implying that the overall rate of adsorption was by chemisorption. By further fitting the equilibrium adsorption data, it was found that the Langmuir isotherm model better describes the mechanism of adsorption process suggesting a single molecular layer adsorption of the adsorbate molecules unto the Zeolite/CeO_2 nanocomposite. In addition, the negative value obtained from the standard Gibb's free energy indicated a spontaneous adsorption process. In the regeneration studies, it was also observed that treating the composite adsorbents with solutions of higher pH values generally gave higher removal efficiencies of the dye molecules during the reuse of the adsorbents.

Acknowledgements

This work is supported through University of Ghana UGRF10 research grant and the Commonwealth Early Academic Fellowship and the Cambridge-Africa Partnership for Research Excellence (CAPREx) Fellowship Programs.

REFERENCES

[1]. Bhatia, D., Sharma, N. R., Singh, J., & Kanwar, R. S. (2017). Biological methods for textile dye removal from wastewater: a review. Critical Reviews in Environmental Science and Technology, 47(19), 1836-1876.

[2]. Holkar, C. R., Jadhav, A. J., Pinjari, D. V., Mahamuni, N. M., & Pandit, A. B. (2016). A critical review on textile wastewater treatments: possible approaches. Journal of environmental management, 182, 351-366.

[3]. Rafatullah, M., Sulaiman, O., Hashim, R., & Ahmad, A. (2010). Adsorption of methylene blue on low-cost adsorbents: a review. Journal of hazardous materials, 177(1-3), 70-80.

[4] Rida, K., Bouraoui, S., & Hadnine, S. (2013). Adsorption of methylene blue from aqueous solution by kaolin and zeolite. Applied Clay Science, 83, 99-105.

[5]. Sherman, J. D. (1999). Synthetic zeolites and other microporous oxide molecular sieves. Proceedings of the National Academy of Sciences, 96(7), 3471-3478.

[6]. Petrov, I., & Michalev, T. (2012). Synthesis of Zeolite A: A Review.

[7]. Koohsaryan, E., & Anbia, M. (2016). Nanosized and Hierarchical Zeolites: A short review. Chinese Journal of Catalysis, 37, 447–467. 10.1016/S1872-2067(15)61038-5

[8]. Eftekhari, S., Habibi-Yangjeh, A., & Sohrabnezhad, S. (2010). Application of Almcm-41 for Competitive Adsorption of Methylene Blue and Rhodamine B: Thermodynamic and Kinetic Studies. Journal of Hazardous Materials, 178, 349-355. 10.1016/j.jhazmat.2010.01.086

[9]. Wang, S., & Peng, Y. (2010). Natural Zeolites as Effective Adsorbents in Water and Wastewater Treatment. Chemical Engineering Journal, 156, 11-24. 10.1016/j.cej.2009.10.029

[10]. Alver, E., & Metin, A.U. (2012). Anionic Dye Removal from Aqueous Solutions using Modified Zeolite: Adsorption Kinetics and Isotherm Studies. Chemical Engineering Journal, 200-202, 59-67.10.1016/j.cej.2012.06.038

[11]. Benkli, Y.E., Can, M.F., Turan, M., & Celik, M.S. (2005). Modification of Organo-Zeolite Surface for the Removal of Reactive Azo Dyes in Fixed-Bed Reactors. Water Research, 39, 487-493. 10.1016/j.watres.2004.10.008

[12]. Esquivel, D., Cruz-Cabeza, A.J., Jimenez-Sanchidrian, C., & Romero-Salguero, F.J. (2013). Transition Metal Exchanged B Zeolites: Characterization of the Metal State and Catalytic Application in the Methanol Conversion to Hydrocarbons. Microporous Mesoporous Materials, 179, 30-39. 10.1016/j.micromeso.2013.05.013

[13]. Goursot, A., Coq, B., & Fajula, F. (2003). Corrigendum to "Toward a Molecular Description of Heterogeneous Catalysis: Transitional Metal Ions in Zeolites. Journal of Catalysis, 216, 324-332. 10.1016/S0021-9517(02)00110-0

[14]. Qi, G., & Yang R.T. (2005). Ultra-Active Fe/ZSM-5 Catalyst for Selective Catalytic Reduction of Nitric Oxide with Ammonia. Applied Catalysis B: Environmental, 60, 13-22. 10.1016/j.apcatb.2005.01.012.

[15]. Razeghi, A., Khodadadi, A., Ziaei-Azad, H., & Mortazavi, Y. (2010). Activity enhancement of Cu-doped ceria by reductive regeneration of CuO– a CeO2 catalyst for preferential oxidation of CO in H2-rich streams. Chemical Engineering Journal, 164(1), 214- 220.

[16]. Tokunaga, S., Haron, M. J., Wasay, S. A., Wong, K. F., Laosangthum, K., & Uchiumi,A. (1995). Removal of fluoride ions from aqueous solutions by multivalent metal compounds. International journal of environmental studies, 48(1), 17-28.

[17]. Pelletier, D. A., Suresh, A. K., Holton, G. A., McKeown, C. K., Wang, W., Gu, B., ... & Brown, S. D. (2010). Effects of engineered cerium oxide nanoparticles on bacterial growth and viability. Applied and environmental microbiology, 76(24), 7981-7989.

[18]. Sawana, R., Somasundar, Y., Iyer, V. S., & Baruwati, B. (2017). Ceria modified activated carbon: an efficient arsenic removal adsorbent for drinking water purification. Applied Water Science, 7(3), 1223-1230.

[19]. Yu, Y., Yu, L., Koh, K. Y., Wang, C., & Chen, J. P. (2018). Rare-earth metal based adsorbents for effective removal of arsenic from water: A critical review. *Critical reviews in environmental science and technology*, *48*(22-24), 1127-1164.

[20]. Nyankson, E., Efavi, J. K., Yaya, A., Manu, G., Asare, K., Daafuor, J., & Abrokwah, R. Y. (2018). Synthesis and characterisation of zeolite-A and Zn-exchanged zeolite-A based on natural aluminosilicates and their potential applications. Cogent Engineering, 5(1), 1440480.

[21]. Li, Y., Du, Q., Liu, T., Sun, J., Wang, Y., Wu, S., ... & Xia, L. (2013). Methylene blue adsorption on graphene oxide/calcium alginate composites. Carbohydrate polymers, 95(1), 501-507.

[22]. Fil, B. A., Ozmetin, C., & Korkmaz, M. (2012). Cationic dye (methylene blue) removal from aqueous solution by montmorillonite. Bulletin of the Korean Chemical Society, 33(10), 3184-3190.

[23]. Zhang, H., Li, X., He, G., Zhan, J., & Liu, D. (2013). Preparation of magnetic composite hollow microsphere and its adsorption capacity for basic dyes. Industrial & Engineering Chemistry Research, 52(47), 16902-16910.

[24]. Qiu, H., Lu, L., Pan, B.-C., Zhang, Q.-J., Zhang, W.-M., & Zhang, Q.-X. (2009). Critical review in adsorption kinetic models. Journal of Zhejiang University SCIENCE A**,** 10, 716-724.

[25]. Y. Ho, G. McKay, Pseudo-second order model for sorption processes, Process Biochem. 34 (1999) 451–465.

[26]. Machado, F. M., Carmalin, S. A., Lima, E. C., Dias, S. L., Prola, L. D., Saucier, C., ... & Fagan, S. B. (2016). Adsorption of Alizarin Red S dye by carbon nanotubes: An experimental and theoretical investigation. The Journal of Physical Chemistry C, 120(32), 18296-18306.

[27]. Tan, I. A. W., Ahmad, A. L., & Hameed, B. H. (2008). Adsorption of basic dye using activated carbon prepared from oil palm shell: batch and fixed bed studies. Desalination, 225, 13-28.

[28]. Langmuir, I. (1918). The adsorption of gases on plane surface of glass, mica and platinum. Journal of the American Chemical Society, 40, 1361-1403. 10.1021/ja02242a004.

[29]. Freundlich, H.M.F. (1906). Uber die adsorption in losungen. Journal of Physical **Chemistry, 57, 385-470.** 10.1515/zpch-1907-5723

[30]. Treacy, M. M., & Higgins, J. B. (2007). Collection of simulated XRD powder patterns for zeolites fifth (5th) revised edition. Elsevier.

[31]. Arumugam, A., Karthikeyan, C., Hameed, A. S. H., Gopinath, K., Gowri, S., & Karthika, V. (2015). Synthesis of cerium oxide nanoparticles using Gloriosa superba L. leaf extract

and their structural, optical and antibacterial properties. Materials Science and Engineering: C, 49, 408-415.

[32]. Goharshadi, E. K., Samiee, S., & Nancarrow, P. (2011). Fabrication of cerium oxide nanoparticles: characterization and optical properties. Journal of colloid and interface science, 356(2), 473-480.

[33]. H.R. Pouretedal, M. Ahmadi, Synthesis, characterization, and photocatalytic activity of MCM-41 and MCM-48 impregnated with CeO2 nanoparticles, Int. Nano Lett. 2(10) (2012) 2-8.

[34]. Mohammadi, T., & Pak, A. (2002). Making zeolite A membrane from kaolin by electrophoresis. Microporous and mesoporous materials, 56(1), 81-88.

[35]. Phokha, S., Pinitsoontorn, S., Chirawatkul, P., Poo-arporn, Y., & Maensiri, S. (2012). Synthesis, characterization, and magnetic properties of monodisperse CeO_2 nanospheres prepared by PVP-assisted hydrothermal method. Nanoscale research letters, 7(1), 425.

[36]. Li, C., Zhong, H., Wang, S., Xue, J., & Zhang, Z. (2015). Removal of basic dye (methylene blue) from aqueous solution using zeolite synthesized from electrolytic manganese residue. Journal of Industrial and Engineering Chemistry, 23, 344-352.

[37]. Moussavi, G., Talebi, S., Farrokhi, M., & Sabouti, R. M. (2011). The investigation of mechanism, kinetic and isotherm of ammonia and humic acid co-adsorption onto natural zeolite. Chemical Engineering Journal, 171(3), 1159-1169.

[38]. Hameed, B. H., Ahmad, A. L., & Latiff, K. N. A. (2007). Adsorption of basic dye (methylene blue) onto activated carbon prepared from rattan sawdust. Dyes and pigments, 75(1), 143-149.

[39]. Seow, T. W., & Lim, C. K. (2016). Removal of dye by adsorption: a review. International Journal of Applied Engineering Research, 11(4), 2675-2679.